Bloch mode scattering matrix methods for modeling extended photonic crystal structures. II. Applications

T. P. White,[1,*] L. C. Botten,[2] C. Martijn de Sterke,[1] R. C. McPhedran,[1] A. A. Asatryan,[2] and T. N. Langtry[2]
[1]*Centre for Ultrahigh-Bandwidth Devices for Optical Systems (CUDOS) and School of Physics, University of Sydney, Sydney, New South Wales 2006, Australia*
[2]*Centre for Ultrahigh-Bandwidth Devices for Optical Systems (CUDOS) and School of Mathematical Sciences, University of Technology, Sydney, New South Wales 2007, Australia*
(Received 8 April 2004; published 15 November 2004)

The Bloch mode scattering matrix method is applied to several photonic crystal waveguide structures and devices, including waveguide dislocations, a Fabry-Pérot resonator, a folded directional coupler, and a Y-junction design. The method is an efficient tool for calculating the properties of extended photonic crystal (PC) devices, in particular when the device consists of a small number of distinct photonic crystal structures, or for long propagation lengths through uniform PC waveguides. The physical insight provided by the method is used to derive simple, semianalytic models that allow fast and efficient calculations of complex photonic crystal structures. We discuss the situations in which such simplifications can be made and provide examples.

DOI: 10.1103/PhysRevE.70.056607 PACS number(s): 42.70.Qs, 02.60.Cb, 42.25.Fx, 42.79.−e

I. INTRODUCTION

In a companion paper [1], hereafter referred to as I, we presented the theoretical framework of the Bloch mode scattering matrix method. In this paper, we build on the results of I and apply the Bloch mode method to the study of several photonic crystal (PC) structures and devices to exhibit the advantages of the method. In I we discussed the full method, based on a complete set of eigenfunctions of the structures, both propagating and evanescent. In implementing the method here, the set of eigenfunctions is truncated at a level determined by the accuracy required in the calculation. We show that in many situations, good results are achieved using an approximate method in which only a few eigenfunctions are included. The choice of which modes to include must be based on the physical properties of the geometry, and, in the cases considered here, they correspond to the propagating modes. The method, in either form, is at its most powerful when the structure consists of a small number of stacks.

The structures we here consider include waveguide dislocations, Fabry-Pérot resonators, a waveguide structure called the "folded directional coupler" (FDC) [2], and a PC-based Y junction. Each of these structures is readily modeled as a finite number of discrete waveguide sections, replicated periodically in the horizontal (x-axis) direction, with propagation occurring in the xy plane. We also demonstrate how the method can provide an intuitive understanding of the underlying physics, leading to simple semianalytic expressions to describe the properties of complex photonic crystal structures. A specific application of this latter approach was discussed in Ref. [3] in the context of a finite photonic crystal waveguide terminated in free space.

*Electronic address: twhite@physics.usyd.edu.au

II. PHOTONIC CRYSTAL AND WAVEGUIDE PARAMETERS

Two-dimensional photonic crystals used for waveguiding typically have square or triangular lattices of cylinders, where the cylinders are either dielectric in an air background, or air cylinders in a dielectric background, and so the refractive index is piecewise constant. Depending on the choice of lattice parameters and refractive index, the PC can have band gaps for TE (magnetic field parallel to cylinder axis) or TM (electric field parallel to cylinder axis) polarization or both. In general, lattices of air cylinders in a background of higher refractive index dielectric have larger TE gaps than TM, and the reverse is the case for dielectric cylinders in air [4].

Two different PC lattices have been chosen for the examples used in this paper. PC1 is a square lattice with period d of dielectric cylinders with refractive index $n_c=3$ in air ($n_b=1$). The cylinder radius is $a=0.3d$, resulting in a TM band gap in the wavelength range $2.986<\lambda/d<3.774$, corresponding to a scaled frequency range of $0.265<\omega d/2\pi c<0.337$. PC2 is a triangular lattice with period d of air cylinders ($n_c=1$) in a dielectric with index $n_b=\sqrt{11.4}$. For a hole radius of $a=0.3d$, a TE band gap exists in the range $3.335<\lambda/d<4.629$ ($0.216<\omega d/2\pi c<0.299$).

To construct the lattices of cylinders for the Bloch mode method described in I, we must first calculate the plane-wave scattering matrices of the individual grating layers that are stacked to produce the lattice. For the Bloch mode analysis, these layers must be periodic with a supercell period D_x, where the unit cell can contain multiple cylinders. Typically, the cylinders in each unit cell are arranged with a local period d, and D_x is chosen to be an integral multiple of the local period, so dislocations are not formed at the edges of the supercell. The supercell period must be large enough to ensure that there is negligible coupling between adjacent cells. For propagation in a straight waveguide in PC1, $D_x>11d$ is sufficient to minimize cross coupling. Thus, un-

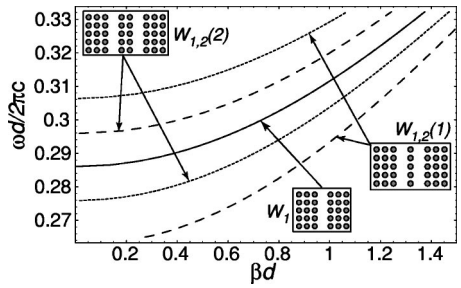

FIG. 1. Dispersion curves for the modes of three straight waveguides formed in photonic crystal PC1. Inset diagrams indicate the waveguide geometry. Dashed lines indicate modes of the double waveguide structures with odd symmetry; dotted lines indicate even modes. The solid curve is the dispersion curve of the single mode of the W_1 waveguide.

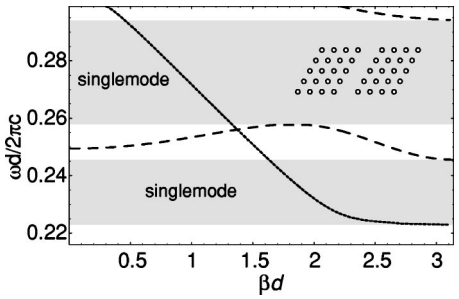

FIG. 2. Dispersion curves for the two modes of a single waveguide in photonic crystal PC2. The dashed curve indicates the mode with odd symmetry, and the dotted curve indicates the even mode. Frequency ranges for singlemode operation are shaded gray.

less otherwise stated, the results given here are for $D_x=21d$, so the structures are essentially isolated from each other. To form a regular photonic crystal, consider stacking many identical grating layers with local period d so that each successive layer is shifted δ_x along the x axis and δ_y along the y axis. Here, the x-y plane lies perpendicular to the axes of the cylinders. Stacking these layers with $\delta_x=0$ and $\delta_y=d$ clearly results in the required geometry for PC1—a square lattice with period d. For reasons to be discussed in Sec. III, it can also be useful to construct the same square lattice with the axes rotated by ±45°. This is achieved by starting with a fundamental grating layer of period $d'=\sqrt{2}d$, corresponding to the separation of cylinders in the Γ-M direction of the lattice. Stacking these layers with $\delta_x=\pm d'/2$ and $\delta_y=d'/2$ results in the same PC1 lattice, but rotated through ±45° in the x-y plane. Similarly, PC2 is constructed by stacking layers with period d such that $\delta_x=\pm d/2$ and $\delta_y=\sqrt{3}/2d$.

Waveguides are formed in a regular photonic crystal lattice by removing lines of one or more cylinders to introduce a localized state within the band gap. Light in one of these "defect modes" cannot propagate within the bulk crystal and thus must propagate along the guide without leaking through the crystal walls. The structures and devices studied in this paper are made up of a small number of different waveguide types. In PC1, a W_1 straight guide can be formed along the Γ-Y crystal axis by removing a single straight line of cylinders as shown in the inset of Fig. 1. The dispersion curve for this guide is shown as a solid curve in Fig. 1, where the propagation constant β is plotted on the horizontal axis and the scaled frequency $\omega d/2\pi c$ is plotted on the vertical axis. Observe that the W_1 guide has a single propagating mode for all frequencies down to the cutoff at $\omega d/2\pi c=0.2865$ ($\lambda=3.49d$).

The second waveguide type that we form in the square lattice is a double waveguide $W_{1,2}(n)$, separated by n lines of cylinders, formed by removing two rows of cylinders as shown in the insets of Fig. 1 for a $W_{1,2}(1)$ and a $W_{1,2}(2)$ guide. The double guide is effectively a coupled pair of W_1 guides, and as such it supports two supermodes $|\psi_\pm\rangle$ of even and odd symmetry, respectively. When n is very large, the two waveguides are effectively isolated from each other, and the propagation constants of the two modes are almost equal ($\beta_+\approx\beta_-$); however, as the guides are brought closer together, this degeneracy is lifted as the fields within the guides interact with each other, and the mode splitting $\Delta\beta=|\beta_+-\beta_-|/2$ increases. The dispersion curves for the modes of a $W_{1,2}(1)$ and a $W_{1,2}(2)$ guide are shown in Fig. 1, with the even modes plotted as dotted curves, and the odd modes as dashed curves. The mode splitting occurs almost symmetrically about the dispersion curve for the single, W_1 guide, and the average propagation constants for the supermodes $\bar{\beta}=|\beta_++\beta_-|/2$ are close to that of the W_1 guide. This property is used in the semianalytic analysis of the folded directional coupler in Sec. V. Note that the mode order is different in the $W_{1,2}(1)$ and the $W_{1,2}(2)$ guides, with the fundamental mode being odd for $n=1$ and even for $n=2$. This issue is discussed in Ref. [5].

When a single cylinder is omitted from each layer of PC2, the resulting waveguide has very different properties to the W_1 guide in PC1. Figure 2 shows the dispersion curves for the propagating modes of the waveguide. As in Fig. 1, the dotted curves represent even modes, and the dashed curves odd modes. Observe, first, that the guide is only single mode in two frequency bands within the band gap, with a second mode existing in the range $0.2455<\omega d/2\pi c<0.2579$, and a third mode at the top of the figure at frequencies higher than $\omega d/2\pi c=0.2942$. Note also that whereas the propagation constant of the first mode increases monotonically with decreasing frequency, the second mode lies between two frequencies, and has a turning point at $\beta\approx1.8$, where its group velocity passes through zero. These properties are in strong contrast to the W_1 waveguide in PC1, which supports no more than one propagating mode, and the dispersion curve of that mode is always positive. The results in Sec. IV for PC2 are all calculated for frequencies in the second band of Fig. 2 ($0.2579<\omega d/2\pi c<0.2942$) where the waveguide is single mode.

III. WAVEGUIDE DISLOCATION

The photonic crystal waveguide is the building block for most photonic crystal devices, and as such, it is essential to characterize its behavior fully. A waveguide formed by a linear defect in an ideal uniform photonic crystal guides light without loss when operated at a frequency where a propagat-

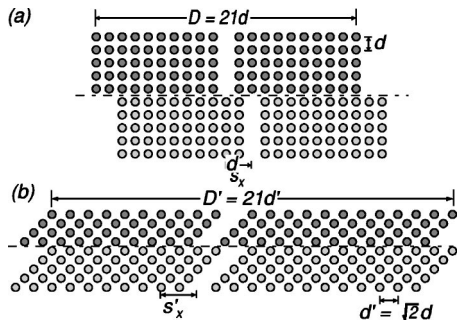

FIG. 3. (a) Straight waveguide with dislocation along the Γ-*X* crystal axis. The circles represent the cross section of the dielectric cylinders forming the 2D photonic crystal. The cylinder shading indicates the two distinct waveguide sections considered in the calculations. (b) Identical waveguide, but with dislocation along the Γ-*M* crystal axis. Both diagrams show the supercell used in the calculations, and the dash-dotted line indicates the line of dislocation. The waveguides extend infinitely in the vertical direction.

ing defect mode exists within the band gap of the crystal. Nonuniformities in the crystal or waveguide structure introduce losses due to reflection and scattering. In this section we consider the effect of a linear dislocation through the crystal and waveguide. Two structures are considered: a dislocation perpendicular to the guide direction (along the Γ-*X* axis of the crystal), as in Fig. 3(a), and a dislocation at a 45° angle to the waveguide (along the Γ-*M* crystal axis) [Fig. 3(b)]. The bulk crystal in Fig. 3(b) is the same square lattice of period d as in 3(a), but rotated by 45°. Thus, when calculating the scattering matrices for the rotated crystal, the lattice period within each grating layer is $d'=\sqrt{2}d$.

The dislocation is modeled as an interface between two identical semi-infinite crystals. To interface two structures with a lateral shift of s_x parallel to the grating layers, we apply a translation operator $\mathbf{Q}_s=\mathrm{diag}[e^{i\alpha_p s_x\sqrt{2}}]$ to the appropriate $\mathbf{R}$ matrices and define $\mathbf{R}_{sx}=\mathbf{Q}_s^{-1}\mathbf{R}\mathbf{Q}_s$. The Fresnel matrices are then calculated as in I, Eqs. (41), with $\mathbf{R}_{sx}$ replacing $\mathbf{R}$. Figure 4 shows the transmission through the dislocated waveguides in Fig. 3 as a function of displacement s_x. The wavelength is fixed at $\lambda=3.25d$. Since the period of the supercell used in these calculations is $D_x=21d$, the transmission curves have the same periodicity.

Most of the features in the spectra of Fig. 4 are easily understood. Both cases exhibit 100% transmission for $s_x=0$,

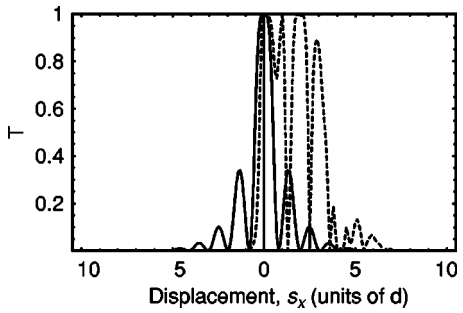

FIG. 4. Transmission of dislocated straight guides, for dislocations parallel to the Γ-*X* (solid curve) and Γ-*M* (dashed curve) crystal axes.

since this corresponds to an infinite guide with no dislocation. However, the two curves show very different behavior when a dislocation is introduced. In the case of the perpendicular dislocation [Fig. 3(a)], the transmission curve is symmetric about $s_x=0$, as expected since the guide is symmetric about the axis transverse to the interface. The monotonically decreasing transmission peaks correspond to peaks in the overlap of the fields in the two waveguide sections. These peaks occur close to integer values of s_x/d since at these points the cylinders in both sections are aligned, and there is no dislocation in the bulk photonic crystal at the interface except at the waveguide ends.

For the 45° dislocation, the transmission curve is strongly asymmetric with respect to the sign of s_x'. This strong asymmetry can be understood from the diagram in Fig. 3(b). When $s_x'>0$ (as in the diagram), the structure resembles two overlapping waveguides at 45° separated by an arrangement of cylinders. In this case, the overlap region allows strong coupling between the two waveguides, and hence strong resonant transmission peaks. For integer values of s_x'/d', the structure resembles the *folded directional coupler* discussed in Sec. V. If the guide is displaced in the $s_x'<0$ direction, however, the two guides are effectively being pulled apart in both directions, and so the transmission is seen to decrease rapidly below 1% and stay low as $|s_x'|$ is increased. Such an asymmetry in transmission with respect to displacement could potentially be used in a sensitive directional motion detector.

IV. FABRY-PÉROT RESONATOR

Resonant devices are an essential component in modern optics, being used in filters, switches, couplers, and many other devices. The Fabry-Pérot (FP) resonator is one of the most basic resonant devices, consisting of two high-reflectivity mirrors on either end of a cavity. Away from resonance, the transmission of the Fabry-Pérot device is typically very small, depending on the reflectivity of the individual mirrors. On resonance, however, the small transmitted amplitude through the first mirror interferes constructively inside the cavity, and high transmission is possible. If the mirrors are identical (balanced), the transmission at resonance can reach 100%, and this is reduced if the reflectivities are unequal. The finesse $\mathcal{F}$ of a balanced FP cavity is defined as the ratio of the fringe separation (free spectral range) to the peak full width at half maximum (FWHM). It is a function of the reflectivity only, given by

$$\mathcal{F}=\pi\sqrt{\mathcal{R}}/(1-\mathcal{R}), \tag{1}$$

where $\mathcal{R}=|r|^2$ is the reflectance of each mirror. Thus, for high-finesse cavities, the mirrors must be strongly reflecting, requiring $\mathcal{R}>0.9985$ for $\mathcal{F}>2000$, assuming there is no loss in the system. We also characterize the resonance by the "quality factor" defined as the ratio of the resonant frequency (ω_0) to the FWHM ($2\Delta\omega_{1/2}$) of the transmission intensity peak, $\mathcal{Q}=\omega_0/(2\Delta\omega_{1/2})$.

Fabry-Pérot devices in photonic crystals have been studied previously in various contexts [6–8]. Here we apply the

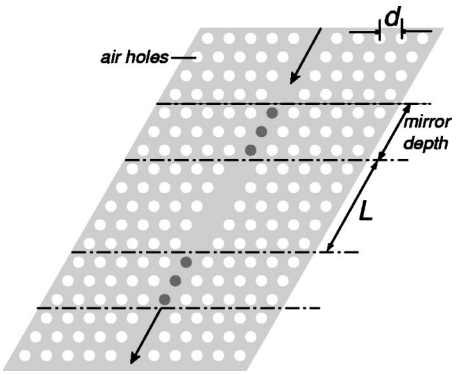

FIG. 5. Diagram of the Fabry-Pérot resonator formed in a single mode waveguide in PC2. The mirrors are formed by "plugs" of cylinders. For the example in this paper, all cylinders are identical.

Bloch mode method to the simple Fabry-Pérot cavity shown in Fig. 5, formed by placing two "plugs" of N_{plug} cylinders in a single mode waveguide formed in the hexagonal PC lattice of air holes, PC2. Although their general behavior is similar to that of conventional Fabry-Pérot resonators, photonic crystal based Fabry-Pérot devices have one significant difference that arises because the mirrors in a photonic crystal FP device are distributed reflectors, with the light penetrating several layers into the crystal structure. This introduces additional spectral features such as resonances in the mirror reflectivity due to reflections within the mirror itself. The reflectivity of the mirrors can be increased by adding more cylinders, or by changing the properties of the cylinders forming the mirror, such as the radius [7]. Figure 6(a) shows the reflectivity of a single mirror as N_{plug} is increased. As expected, the reflectivity increases with the number of cylinders; however, the effect is not monotonic at all wavelengths due to resonant reflections from either end of the plug. Adjusting the radius or the refractive index of the plug cylinders can also result in improved or degraded reflection from the mirror.

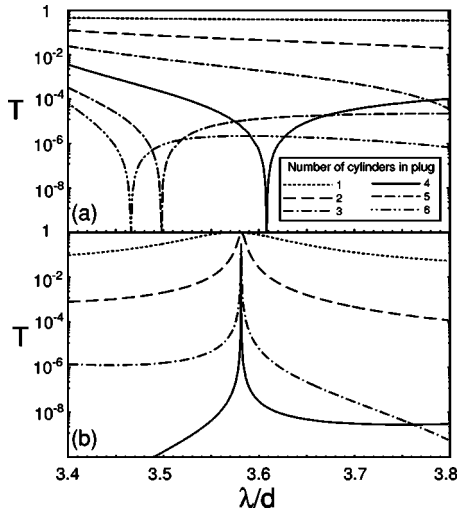

FIG. 6. (a) Transmission (log scale) as a function of normalized wavelength, through a single mirror (plug) formed in a single mode waveguide in PC2 for mirrors with $N_{\text{plug}}=1-6$. (b) Transmission through Fabry-Pérot cavity of length $L=5d$ in the single mode waveguide for mirrors with $N_{\text{plug}}=1-4$. The legend inset in (a) applies to the line styles in both (a) and (b).

The properties of an individual mirror can be calculated with the Bloch mode method as a three-section waveguide structure, where the two end sections are identical single waveguides, and the central section is composed of complete layers of cylinders (possibly with changes made to the central one). The transmission and reflection is then calculated using

$$\mathsf{R} = \mathsf{R}_{12} + \mathsf{T}_{21}\mathbf{\Lambda}^{L}\mathsf{R}_{23}\mathbf{\Lambda}^{L}(\boldsymbol{I} - \mathsf{R}_{21}\mathbf{\Lambda}^{L}\mathsf{R}_{23}\mathbf{\Lambda}^{L})^{-1}\mathsf{T}_{12},$$

$$\mathsf{T} = \mathsf{T}_{23}\mathbf{\Lambda}^{L}(\boldsymbol{I} - \mathsf{R}_{21}\mathbf{\Lambda}^{L}\mathsf{R}_{23}\mathbf{\Lambda}^{L})^{-1}\mathsf{T}_{12}, \qquad (2)$$

where the subscripts in the expressions on the right hand side define the interface and the direction of incident light. Equations (2) follow directly from Eqs. (54) in I by choosing $N=3$. Here, propagation between the two interfaces is described by the Λ matrices which contain the eigenvalues μ corresponding to the Bloch modes of the central waveguide section of length L.

The scattering matrices in Eq. (2) are calculated for each of the interfaces, with any symmetries being taken into account to save computation time. In this case the mirror is symmetric with identical waveguides on both sides, so $\mathsf{T}_{21}=\mathsf{T}_{23}$ and $\mathsf{R}_{21}=\mathsf{R}_{23}$, giving a significant reduction in the required scattering matrix calculations. Many calculations can benefit from an understanding of the symmetry properties of the structure as we show in the examples throughout this paper.

Unless the central blocking cylinder is made very small, the plug section does not support any propagating modes, and hence the reflection of the propagating modes at the 1-2 interface is 100%. However, the mirror is of finite thickness so energy can be coupled through the plug between the two waveguides by evanescent modes, giving a nonzero transmission of the propagating Bloch mode from section 1 to section 3.

The FP cavity is formed by placing two of these mirrors in a length of single mode waveguide, with a separation of length Ld. Using the scattering matrices for the mirrors at each end as the new interface scattering matrices, we now consider the three sections to be the composite mirrors at each end (sections 1 and 3) and the central waveguide of length L (section 2). Transmission through the whole FP structure is calculated once again as that through a three-layer structure using Eqs. (2). Figure 6(b) shows the transmission spectra for a cavity of length 5 with increasing mirror thickness. As expected from Eq. (1), the peak width becomes narrower ($\mathcal{Q}$ increases) as the reflectivity of the mirrors is increased. In this case, since the reflectivity of the mirrors increases exponentially with N_{plug} at most wavelengths [see Fig. 6(a)], $\mathcal{Q}$ also increases very rapidly with the size of the mirror. Table I shows the quality factor of the Fabry-Pérot resonance as a function of the number of cylinders in the mirror.

The results above include both propagating and evanescent Bloch mode orders. It is not always necessary, however, to include the evanescent orders and in these cases, many of

TABLE I. Resonant wavelength (units of d), $\mathcal{Q}$, and $\mathcal{F}$ for a simple Fabry-Pérot cavity in PC2 for increasing mirror thickness. Resonant wavelength and $\mathcal{Q}$ values are given for both the full numerical calculation (full) and the propagating model analysis result (prop).

N_{plug}	$\lambda_0(d)$ (full)	$\lambda_0(d)$ (prop)	$\mathcal{Q}$ (full)	$\mathcal{Q}$ (prop)	$\mathcal{F}\ [=\pi\sqrt{\mathcal{R}}/(1-\mathcal{R})]$
1	3.686 92	3.686 92	78	78	6.8
2	3.690 90	3.690 91	1200	1200	97
3	3.690 642	3.690 656	6.6×10^4	6.4×10^4	5.4×10^3
4	3.690 597 4	3.690 610 8	1.3×10^6	1.1×10^6	1.1×10^5

the complicated matrix expressions can be replaced with semianalytic scalar forms [3]. For the FP cavity described above, the mirror sections have no propagating modes, thus relying on evanescent modes to carry energy through the reflecting layers into the cavity. Between the mirrors, however, most of the energy is carried by the single propagating Bloch mode, suggesting that a propagating mode analysis might be appropriate. Here we outline an asymptotic analysis that can be applied to a general class of PC structures that comprise three distinct media M_1, M_2, and M_3 with the first and last of these being semi-infinite in extent, and the second M_2 having a finite length of L layers.

For such structures, the Bloch mode reflection and transmission matrices are given by Eq. (2). Now, if media M_1 and M_3 are identical and medium M_2 is shrunk to a degenerate length of $L=0$, it follows on physical grounds that $\mathsf{R}=0$ and $\mathsf{T}=\boldsymbol{I}$. From these relationships, we may deduce $\mathsf{T}_{12}\mathsf{T}_{21}=\boldsymbol{I}-\mathsf{R}_{21}^2$ and also that $\mathsf{R}_{12}\mathsf{T}_{21}+\mathsf{T}_{21}\mathsf{R}_{21}=0$, both of which hold analytically within the formulation.

In the case of a photonic crystal structure M_2 which is terminated at each end by (M_1) (e.g., a waveguide terminated at each end in free space [3]), these relationships give

$$\mathsf{R}=\mathsf{T}_{12}^{-1}(-\mathsf{R}_{21}+\boldsymbol{\Lambda}^L\mathsf{R}_{21}\boldsymbol{\Lambda}^L)(\boldsymbol{I}-\mathsf{R}_{21}\boldsymbol{\Lambda}^L\mathsf{R}_{21}\boldsymbol{\Lambda}^L)^{-1}\mathsf{T}_{12},$$

$$\mathsf{T}=\mathsf{T}_{12}^{-1}(\boldsymbol{I}-\mathsf{R}_{21}^2)\boldsymbol{\Lambda}^L(\boldsymbol{I}-\mathsf{R}_{21}\boldsymbol{\Lambda}^L\mathsf{R}_{21}\boldsymbol{\Lambda}^L)^{-1}\mathsf{T}_{12},$$

which we recognize as generalizations of the Airy formulae [9] for a Fabry-Pérot interferometer.

The most significant advantage in using Bloch mode methods derives from their capacity to efficiently handle long propagation spans in a fixed medium. Since this is characterized by the matrix $\boldsymbol{\Lambda}^L$, it follows that for sufficiently long spans (typically $L>5$ or more), the evanescent modes can be disregarded, with all calculations dominated by the propagating states. We thus consider an asymptotic analysis in the case of a single propagating mode for which $\boldsymbol{\Lambda}^L \simeq \boldsymbol{w}\mu^L\boldsymbol{w}^H$ where $\boldsymbol{w}$ is a row vector $[1\ 0\ 0\ldots0]^T$, and μ^L is a scalar representing the propagating constant across the L layers of M_2. Multimode structures can be handled similarly, with $\boldsymbol{w}$ containing additional columns of the unit matrix and μ^L being a diagonal matrix containing the propagating eigenvalues μ_i^L [10].

In response to an incident field (in M_1) characterized by the mode vector $\boldsymbol{\delta}$, the transmitted field is then

$$\begin{aligned}\boldsymbol{t} &= \mathsf{T}_{23}\boldsymbol{\Lambda}^L(\boldsymbol{I}-\mathsf{R}_{21}\boldsymbol{\Lambda}^L\mathsf{R}_{23}\boldsymbol{\Lambda}^L)^{-1}\mathsf{T}_{12}\boldsymbol{\delta}\\ &= \mathsf{T}_{23}\boldsymbol{w}\mu^L(\boldsymbol{I}-\boldsymbol{w}^H\mathsf{R}_{21}\boldsymbol{w}\mu^L\boldsymbol{w}^H\mathsf{R}_{23}\boldsymbol{w}\mu^L)^{-1}\boldsymbol{w}^H\mathsf{T}_{12}\boldsymbol{\delta}\\ &= (\mathsf{T}_{23}\boldsymbol{w}\boldsymbol{w}^H\mathsf{T}_{12}\boldsymbol{\delta})\frac{\mu^L}{1-\rho^2\mu^{2L}},\end{aligned} \tag{3}$$

resulting from the application of the Woodbury formula [11], where $\rho=\boldsymbol{w}^H\mathsf{R}_{21}\boldsymbol{w}$. The transmitted flux is then

$$\mathcal{E}_f=\boldsymbol{t}^H\boldsymbol{\mathcal{I}}_3\boldsymbol{t}=\frac{|\boldsymbol{w}^H\mathsf{T}_{12}\boldsymbol{\delta}|^2}{|1-\rho^2\mu^{2L}|^2}\boldsymbol{w}^H\mathsf{T}_{23}\boldsymbol{I}_3\mathsf{T}_{23}\boldsymbol{w}. \tag{4}$$

From the energy conservation relationships in I [Sec. II B, Eq. (44)], we realize

$$\mathsf{T}_{23}\boldsymbol{I}_3\mathsf{T}_{23}=\boldsymbol{I}_2-\mathsf{R}_{23}\boldsymbol{I}_2\mathsf{R}_{23}+i\mathsf{R}_{23}^H\boldsymbol{I}_2^- - i\boldsymbol{I}_2^-\mathsf{R}_{23},$$

and since $\boldsymbol{I}_2=\boldsymbol{w}\boldsymbol{w}^H$, it follows that $\mathbf{w}^H\mathsf{T}_{23}\boldsymbol{I}_3\mathsf{T}_{23}\boldsymbol{w}=1-|\rho|^2$. Thus, the energy flux propagating through the structure is

$$\mathcal{E}_f=\frac{1-|\rho|^2}{|1-\rho^2\mu^{2L}|^2}|\boldsymbol{w}^H\mathsf{T}_{12}\boldsymbol{\delta}|^2. \tag{5}$$

Here, the denominator represents the interferometric action of the devices, while the numerator expresses the net downward transmission of the flux associated with the single propagating mode.

To apply this asymptotic treatment to the the Fabry-Pérot resonator in Fig. 5, we first calculate the transmission and reflection matrices through a single mirror using the full Bloch mode calculation. These Bloch mode Fresnel matrices can then be substituted into the result of Eq. (3) as T_{23} and T_{12} and R_{12}, along with the eigenvalue μ for the single propagating mode of the waveguide. The resulting scalar equation gives the transmission through the complete FP structure as a function of the cavity length L. Since the properties of the mirror are wavelength dependent, the scattering matrices must be calculated for each wavelength of interest. In practice, only the single element of each scattering matrix corresponding to the propagating mode needs to be saved once the matrix has been calculated.

The effect of neglecting the evanescent modes within the cavity can be seen in Table I, where the resonant wavelength and $\mathcal{Q}$ for the FP cavity of length $5d$ are compared for the full evanescent field calculation and the reduced, propagating mode calculation. For all but the highest-$\mathcal{Q}$ cavities, the agreement is excellent. If the cavity length is reduced, it might be expected that the evanescent fields would have a more significant effect on the results. However, even for cav-

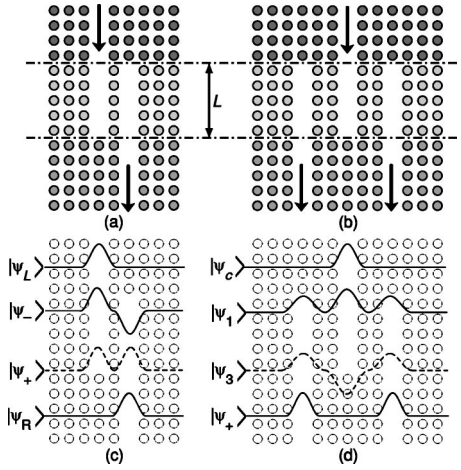

FIG. 7. (a) Geometry of the FDC and (c) schematics of the propagating modes in each of the three sections. All of the cylinders are identical, and the shading is to emphasize the three distinct waveguide sections. (b) Geometry of the coupled Y junction and (d) schematics of the propagating modes of even symmetry.

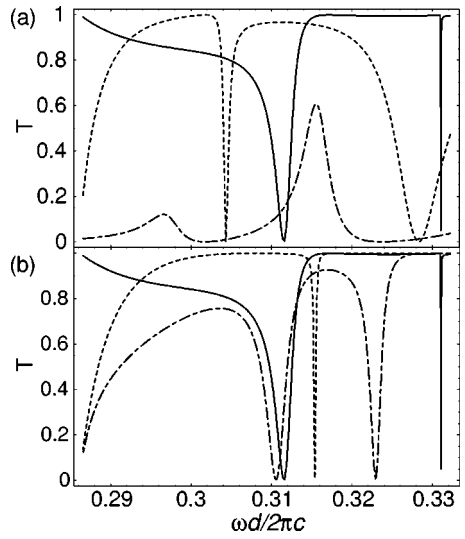

FIG. 8. FDC transmission spectra for (a) FDC of length $L=5d$ with guide separations of $N_c=1$ (solid), $N_c=2$ (dashed), and $N_c=3$ (dash-dotted) and (b) FDC with $N_c=1$ and cavity lengths $L=4$ (dashed), $L=5$ (solid), and $L=6$ (dash-dotted).

ity lengths of two lattice periods, the difference between the propagating mode result and the full result is relatively small. For mirrors that are three layers thick, the difference in resonant frequency calculated with the two methods is less than 0.05%, and the $\mathcal{Q}$ values agree to two figures. Table I also shows the finesse calculated using the standard FP equation (1) and the reflectivity $\mathcal{R}=|\rho|^2$ as plotted in Fig. 6(a).

We have demonstrated one method for changing the finesse of a simple Fabry-Pérot cavity, but many alternative approaches could be taken to design optimized devices for specific operations. For example, the plug cylinders could be individually tuned [7] for a specific finesse and/or resonant frequency, or even dynamically tuned using thermo-optic effects to produce a tunable device.

V. FOLDED DIRECTIONAL COUPLER

Recently [2] we reported on a design for a compact PC-based resonant filter, the folded directional coupler. This device makes use of mode coupling between two parallel waveguides, as in a directional coupler, and Fabry-Pérot resonances due to multiple reflections within a cavity region. The parameters reported in Ref. [2] were for a FDC of length $5d$ that behaved as a notch-rejection filter with $Q>10^4$. The transmission properties are complementary to those of a Fabry-Pérot cavity, with almost 100% transmission away from resonance, and almost 100% reflection at the resonant frequency.

As shown in Fig. 7, the FDC structure is simply two semi-infinite single mode waveguides with a common coupling region of length L where the guides run parallel to each other, separated by N_c lines of cylinders. Within the cavity region, the modes of the two guides couple as in a directional coupler to form supermodes that allow energy to transfer between the guides. At each end of the cavity, one of the waveguides is closed, and the other is open. Reflections from the closed guide reflect some of the light back into the cavity, while some light is transmitted out of the cavity into the open guide. Multiple reflections from the closed guide ends result in strong resonant behavior as in a Fabry-Pérot cavity. In terms of modeling the FDC structure with the Bloch mode method, we consider it to consist of three distinct waveguide sections: (1) a single mode input guide of type W_1 aligned to one of the guides of (2) a double waveguide of type $W_{1,2}(N_c)$, where the guides are separated by N_c rows of cylinders, and (3) an output guide also of type W_1 aligned with the other guide to the input.

In general, FDC structures exhibit quite a complicated and varied range of transmission spectra. Several examples are shown in Fig. 8, where the transmission is plotted as a function of frequency for different guide separations (a) and cavity lengths (b). The solid curve in both graphs of Fig. 8 is for a cavity length of $L=5d$ and guide separation of $N_c=1$. It clearly shows the resonance at $\omega d/2\pi c=0.3311$ which was used to design the filter device described in Ref. [2].

In Ref. [2], an analytic expression was given that was derived from simple mode coupling and reflection arguments that only require numerical input of the propagation constants of the two supermodes within the cavity. The expression can also be derived by starting with the full Bloch mode method, and making the same type of approximations. The first approximation is to reduce the size of the Bloch mode scattering matrices to include only the propagating modes in each section of the FDC: a single mode in the input guide, a single mode in the output guide, and two modes in the central double guide section. Figure 7(c) shows schematics of mode profiles in each waveguide section. At the first interface, the single mode couples into the supermodes of the double guide. Ignoring the back reflection at this first interface since the input guide essentially continues into the double guide section, we can write approximate expressions for the Bloch mode reflection and transmission matrices

$$\mathsf{R}_{12}=0, \quad \mathsf{T}_{12}=\begin{pmatrix} \frac{1}{\sqrt{2}} & \frac{-1}{\sqrt{2}} \end{pmatrix} \tag{6}$$

where we have used the approximation that a mode in the input guide (left) can be approximated by $|\psi_L\rangle=(|\psi_+\rangle - |\psi_-\rangle)/\sqrt{2}$. This assumption is valid if the mode of the single waveguide is not significantly distorted by the presence of the second, parallel waveguide. At the interface between the double guide and the output guide, we again assume that the mode in the open guide $[|\psi_R\rangle=(|\psi_+\rangle+|\psi_-\rangle)/\sqrt{2}]$ [see Fig. 7(c)] is transmitted freely into the output guide, and so we can write $\mathsf{T}_{23}=(1/\sqrt{2}\ 1/\sqrt{2})$. The reflection matrix at the second interface is a 2×2 matrix, where element (i,j) is the reflection coefficient for the reflection of mode j into mode i (traveling in the opposite direction), and modes 1 and 2 are the even and odd supermodes, respectively. Once again, assuming that a mode in the right guide is completely transmitted while a mode in the left guide is completely reflected back into the left guide, we can write

$$\mathsf{R}_{23}\cdot\begin{pmatrix} \frac{1}{\sqrt{2}} & \frac{1}{\sqrt{2}} \\ -\frac{1}{\sqrt{2}} & \frac{1}{\sqrt{2}} \end{pmatrix}=\begin{pmatrix} \frac{1}{\sqrt{2}} & 0 \\ -\frac{1}{\sqrt{2}} & 0 \end{pmatrix} \Rightarrow \mathsf{R}_{23}=\begin{pmatrix} \frac{1}{2} & -\frac{1}{2} \\ -\frac{1}{2} & \frac{1}{2} \end{pmatrix}. \tag{7}$$

Similar arguments are used to find the final scattering matrix,

$$\mathsf{R}_{21}=\begin{pmatrix} \frac{1}{2} & \frac{1}{2} \\ \frac{1}{2} & \frac{1}{2} \end{pmatrix}. \tag{8}$$

The simplified scattering matrices are then substituted into the generalized Fabry-Pérot equation (2) for the three-layer structure. The $\mathbf{\Lambda}$ term representing propagation through the central section of the structure is a 2×2 diagonal matrix of the eigenvalues $\mu_j=\exp(i\bar{\beta}_j d)$, where $j=1, 2$.

Following substitution of $\bar{\beta}$ and $\Delta\beta$ as defined in Sec. II, the following expressions for the complex transmission and reflection of the FDC structure are derived:

$$\mathsf{R}=\frac{\cos^2(\Delta\beta L)\exp(2i\bar{\beta}L)}{1+\sin^2(\Delta\beta L)\exp(2i\bar{\beta})L}$$

$$\mathsf{T}=i\exp(i\bar{\beta}L)\sin(\Delta\beta L)\frac{1+\exp(2i\bar{\beta}L)}{1+\sin^2(\Delta\beta L)\exp(2i\bar{\beta}L)}. \tag{9}$$

These equations are identical to those derived under the same assumptions from the simple mode coupling and reflection model, described in Ref. [2]. Given that the derivations are from quite different approaches, it is pleasing that the resulting formulas are identical. The treatment outlined here has advantages over the coupling model, in that it provides a systematic approach that is more easily applicable to complicated structures.

Equations (9) require the numerical input of $\Delta\beta$ and $\bar{\beta}$, and these must be calculated with a numerical method. Here, we use the full Bloch method to calculate the propagation constants of the supermodes. The other input parameter is the cavity length, L. Although L has been defined previously as the number of complete layers making up the double guide region, this is not necessarily the correct value to use in Eq. (9), since the guide ends act as distributed reflectors, and the phase on reflection is a function of wavelength. The transmission spectra calculated from Eq. (9) do have very similar shapes to those of the full transmission calculation, and with some adjustment of L from the integer value, the curves can be matched with reasonable accuracy. Attempts to correct L to give the correct phase on reflection have proved to be no more accurate than the simple result which assumes that $r=1$ at the end of a guide.

An intermediate approach between the full Bloch mode calculation and the simplified approach above can also be used to obtain accurate results more efficiently. The scattering matrices can be cut back after they have been calculated to include only the propagating modes, reducing them to the same dimensions as the idealized versions in Eqs. (6)–(8). The elements of the scattering matrices in this case, however, include accurate amplitude and phase information. This approximation is excellent for most FDC structures and the smaller matrices greatly reduce subsequent calculation requirements.

Simplified semianalytic expressions such as those given here are very useful for quickly examining new FDC structures, requiring only the calculation of $\Delta\beta$ and $\bar{\beta}$. They also provide an intuitive understanding of the FDC properties, such as the very high-Q resonances exploited in Ref. [2]. A very powerful and efficient set of design tools is created when such semianalytic methods are combined with more accurate numerical approaches like the full Bloch mode method.

VI. COUPLED Y JUNCTION

Efficient, wide-bandwidth Y junctions or beam splitters are required for compact integration of multiple optical devices on photonic chips. As a basic component of many integrated optical devices, these junctions must be designed with a minimum back reflection and maximum transmission over the operating bandwidth. A number of studies have been made into the optimal method of splitting a single guided mode into two modes, and the approaches taken can be broadly classified into two groups. The first design approach has been to optimize simple Y-junction designs, while the second approach has been to design alternative structures exploiting the properties of photonic crystals. Good transmission has been demonstrated in Y junctions both theoretically [12–14] and experimentally [14] using optimization techniques such as placing one, or several, "tuning" cylinders near the junction of three waveguides. High-transmission junctions, with calculated transmissions up to 99% have been designed; however, in most cases, the transmission bandwidth decreases rapidly as the maximum transmission approaches 100% [12]. Typical bandwidths for the

devices reported in the literature in triangular lattice PC structures with air holes are on the order of 10–40 nm for 95% transmission.

An alternative to the Y junction is essentially a directional coupler with the length chosen to be half of the coupling length, ensuring that light incident in one of the guides is split evenly between the two guides. Such a structure was proposed in Ref. [15] as a means of splitting an input beam for a Mach-Zehnder interferometer application. The optimal coupling length is wavelength dependent, but may be robust enough to give a satisfactory bandwidth. One of the big advantages of a coupler-based beam splitter is that the back reflection can be negligible. Variations in coupler length affect the splitting ratio in the output guides, but do not affect the total transmission of the splitter. This is an important issue in compact devices where back reflections can cause unwanted interference effects.

Here, we present a coupled Y-junction design that operates similarly to a coupled beam splitter, but with the symmetry properties of a Y junction, which ensure the transmission into each output arm is identical. We show that the device is also very closely related to the folded directional coupler, and a modal analysis similar to that in Sec. V yields identical expressions for the transmission and reflection. The general geometry of the coupled Y junction is illustrated in Fig. 7(b). Observe that the single input guide enters a region where it lies beside the two output guides, as in the FDC, or a directional coupler. Light entering the triple guide region in the central waveguide couples to the two guides on either side. If the length of the triple guide region is such that all of the light has been transferred into the outer guides at the far end of the triple guide region, then almost all light propagates into the two output guides. The separation of the output guides in this particular design is only five lattice periods; however, calculations show that the coupling length of the modes in the two output guides is several hundred lattice periods. For compact devices, the output guides can therefore be considered isolated from each other.

A simple analysis of the coupled Y junction can proceed in an almost identical manner to the FDC structure. We must first consider the propagating modes within each of the three regions. The input guide has been chosen to support a single mode, which has even symmetry with respect to the center of the guide. The output guides support two modes, with odd and even symmetry, and the central triple guide region can support three modes—two with even symmetry and one with odd symmetry. The structural symmetry of the device, and the fact that the input waveguide can support only an even mode, mean that there is never any coupling of energy into the odd modes of either the triple guide or the double guide regions. Thus, we have a single input mode coupling into two modes in the central region, which then couple into a single mode in the output guides, in much the same way as in the FDC. Schematics of the even modes in each region of the coupled Y junctions are shown in Fig. 7(d).

Following the analysis of Sec. V, we consider the supermodes of the multiple guide regions to be a superposition of modes localized in each guide. For the triple guide region, denote fields in each of the right, central, and left guides as $|\psi_L\rangle, |\psi_C\rangle$, and $|\psi_R\rangle$, respectively. The three supermodes can then be approximated by [16]

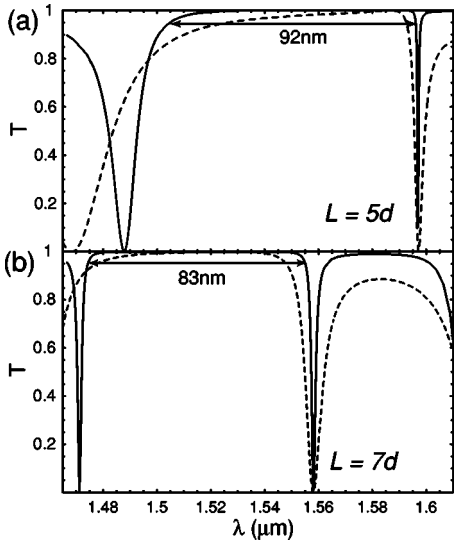

FIG. 9. Transmission curves for the coupled Y junction with lengths (a) $L=5d$ and (b) $L=7d$. Wavelengths have been scaled so that the high-transmission bands occur near $\lambda=1.55$ μm. The 95% transmission bandwidths are 92 and 83 nm, respectively.

$$|\psi_1\rangle = \frac{1}{2}(|\psi_L\rangle + \sqrt{2}|\psi_C\rangle + |\psi_R\rangle),$$

$$|\psi_2\rangle = \frac{\sqrt{2}}{2}(|\psi_L\rangle - |\psi_R\rangle),$$

$$|\psi_3\rangle = \frac{1}{2}(|\psi_L\rangle - \sqrt{2}|\psi_C\rangle + |\psi_R\rangle),$$

where modes 1 and 3 have even symmetry, and mode 2 has odd symmetry. We approximate the propagation constants of these modes by $\beta_1=\bar{\beta}+\Delta\beta$, $\beta_2=\bar{\beta}$, and $\beta_3=\bar{\beta}-\Delta\beta$, where $\bar{\beta}=(\beta_1+\beta_2)/2$ and $\Delta\beta=(\beta_1-\beta_2)/2$. Note that the analysis here is unaffected by the order of the supermodes of the coupled waveguides [10]. The direct mapping to the FDC occurs because the input mode can be written as $|\psi_C\rangle = (|\psi_1\rangle - |\psi_3\rangle)/\sqrt{2}$ and the even supermode in the double output guide as $|\psi_+\rangle = (|\psi_1\rangle + |\psi_3\rangle)/\sqrt{2}$. As stated above, no light couples to the odd modes in the triple guide or the double output guide, and so we can ignore them in the analysis. The final expressions for the transmission and reflection of the coupled Y junction are thus identical to Eq. (9) with $\bar{\beta}$ and $\Delta\beta$ calculated for the modes of the triple guide, rather than the double guide.

Although the coupled Y junction also exhibits the sharp resonances of the FDC, it is the flat-topped, high-transmission regions of the spectrum that we wish to exploit for the purposes of this device. Figures 9(a) and 9(b) show the transmission through two different coupled Y-junctions, with lengths $L=5d$ and $L=7d$, respectively. The junction has been formed in the PC1 lattice, with the output guides separated by five rows of cylinders, and each of the guides in the central region separated by two rows of cylinders. For lengths of $L=5d$ and $L=7d$, the Y junction has 95% trans-

mission bandwidths of approximately 92 and 83 nm, respectively at $\lambda = 1.55$ μm, and 99% transmission bandwidths of about 80 and 76 nm. The dashed curves in Figs. 9(a) and 9(b) show the result of the analytic expression (9) for the coupled Y-junction transmission with $L = 5.75$ and $L = 7.80$, respectively, for the two devices. The solid curves show the transmission calculated using the full Bloch mode method. The difference in the physical length and the length parameter in the model is a result of phase changes upon reflection, and the difficulty in defining a reflection plane at either end of the triple guide region. The analytic results were used to predict the most suitable geometry for the junction, and it can be seen that the transmission bandwidth obtained from the full Bloch mode calculation is better than the analytic model suggests.

When designing the coupled Y junction for maximum bandwidth, the splitting of the modes in the triple guide region must be considered. Since the successful operation of the device requires two propagating even modes to exist in this region, we must operate in the frequency range above the cutoff of the second even mode, and below the high-frequency edge of the band gap. If the three guides are too close together, the mode splitting becomes very large, and the frequency range for operation becomes limited. If the guides are too far apart, the mode splitting becomes so small that the coupling length required for light to couple from the central guide to the outer guides becomes very large. Thus, the choice of guide separation and its effect on mode splitting must be considered. It is expected that the bandwidths could be further increased by adjusting either the radius or the refractive index of the cylinders between the guides to tune $\Delta\beta$ and $\overline{\beta}$ for optimum performance. In the examples chosen above, the second even mode cutoff occurs at $\lambda \approx 3.32d$, giving a maximum bandwidth of $\Delta\lambda = 0.33d$ corresponding to approximately 160 nm at $\lambda = 1.55$ μm.

The coupled Y-junction design provides a solution to the problem of achieving high-transmission, wide-bandwidth beamsplitting. Such properties make this junction ideal for use in PC-based Mach-Zehnder interferometers [17], where high-performance junctions are required. Further work will be required to determine how the performance of such a junction compares to more conventional Y-junction designs, not only in terms of transmission and bandwidth, but also regarding tolerance to fabrication and material variations.

VII. CONCLUSION

The examples presented in this paper are chosen to demonstrate the flexibility of the Bloch mode method for calculating properties of photonic crystal waveguide devices and circuits. As a full numerical tool, the method is fast and efficient as it relies on representing devices as stacks of distinct photonic crystal waveguide sections. The interface between each pair of waveguides is characterized by a set of generalized Fresnel scattering matrices which describe the reflection and transmission of the Bloch modes (both propagating and evanescent) within each waveguide section. As we have shown, it can lead to simple expressions for device performance which enhance physical understanding and facilitate efficient optimization.

A limitation of the method lies in the enforced periodicity introduced by the supercell approach. The advantage of this approach is that it is sufficient to deal with a discrete set of plane wave orders to couple the fields in adjacent gratings. The method works well for frequencies inside a photonic band gap, as then the superperiod can always be taken to be sufficiently large to isolate, in effect, the different cells. However, for frequencies in one of the bands, the light can propagate in the transverse direction and the effective isolation is much more challenging.

Though the method can be applied to any problem to which a supercell can be applied, it is most efficient when two conditions are satisfied. The first of these is the need for a limited number of relevant modes so that an analytic or semianalytic approach is feasible. As we discussed in Sec. V, a hybrid method, in which reflection or transmission matrices of low dimension are obtained from a rigorous calculation, may be preferable. In addition to this, the efficiency of the method also improves when the structure under consideration consists of only a few different types of gratings. In this case the transmission and reflection matrices of only a few different gratings, the most intensive part of the calculation, need to be determined.

ACKNOWLEDGMENTS

This work was produced with the assistance of the Australian Research Council under the ARC Centres of Excellence program.

[1] L. C. Botten, T. P. White, A. A. Asatryan, T. N. Langtry, C. M. de Sterke, and R. C. McPhedran, preceding paper, Phys. Rev. E **70**, XXXXXX (2004).
[2] T. P. White, L. C. Botten, R. C. McPhedran, and C. M. de Sterke, Opt. Lett. **28**, 2452 (2003).
[3] L. C. Botten, A. A. Asatryan, T. N. Langtry, T. P. White, C. M. de Sterke, and R. C. McPhedran, Opt. Lett. **28**, 854 (2003).
[4] J. Joannopoulos, R. Meade, and J. Winn, *Photonic Crystals* (Princeton University, Princeton, NJ, 1995).
[5] C. M. de Sterke, L. C. Botten, A. A. Asatryan, T. P. White, and R. C. McPhedran, Opt. Lett. **29**, 1384 (2004).
[6] M. Koshiba, Y. Tsuji, and M. Hikari, J. Lightwave Technol. **18**, 102 (2000).
[7] R. Costa, A. Melloni, and M. Martinelli, IEEE Photonics Technol. Lett. **15**, 401 (2003).
[8] A. S. Jugessur, P. Pottier, and R. M. De La Rue, Opt. Express **12**, 1304 (2004).
[9] M. Born and E. Wolf, *Principles of Optics*, 5th ed. (Pergamon, Oxford, 1975).
[10] L. C. Botten, T. P. White, C. M. de Sterke, R. C. McPhedran,

A. A. Asatryan, and T. N. Langtry, Opt. Express **12**, 1592 (2004)
[11] W. H. Press, S. A. Teukolsky, W. T. Vetterling, and B. P. Flannery, *Numerical Recipes in FORTRAN 77* (Cambridge University Press, Cambridge, England, 1997).
[12] S. Boscolo, M. Midrio, and T. F. Krauss, Opt. Lett. **27**, 1001 (2002).
[13] W. J. Kim and J. D. O'Brien, J. Opt. Soc. Am. B **21**, 289 (2004).
[14] R. Wilson, T. J. Karle, I. Moerman, and T. F. Krauss, J. Opt. A, Pure Appl. Opt. **5**, S76 (2003).
[15] A. Martinez, A. Griol, P. Sanchis, and J. Marti, Opt. Lett. **28**, 405 (2003).
[16] P. Yeh, *Optical Waves in Layered Media* (Wiley, New York, 1988).
[17] T. P. White, C. M. de Sterke, R. C. McPhedran, T. Huang, and L. C Botten, Opt. Express **12**, 3035 (2004).